Anodic dissolution of metals in oxide-free cryolite melts

Laurent Cassayre, Pierre Chamelot, Laurent Arurault, Pierre Taxil

Anodic dissolution of metals in oxide-free cryolite melts

L. CASSAYRE[1,2,*], P. CHAMELOT[1], L. ARURAULT[3] and P. TAXIL[1]
[1]*Laboratoire de Génie Chimique (LGC), Université Paul Sabatier, UMR 5503, 118 route de Narbonne, 31062 Toulouse Cedex 04, France*
[2]*Alcan, Voreppe Research Center, 725 rue Aristide Bergès, 38341 Voreppe, France*
[3]*Centre Interuniversitaire de Recherche et d'Ingénierie des Matériaux (CIRIMAT), Université Paul Sabatier, UMR 5085, 118 Route de Narbonne, 31062 Toulouse, Cedex 04, France*
*(*author for correspondence, tel.: +33-561-55-7465, fax: +33-561-55-6139, e-mail: laurent_cassayre@yahoo.fr)*

Key words: anodic dissolution, cryolite, fluorine evolution

Abstract

The anodic behavior of metals in molten cryolite-alumina melts has been investigated mostly for use as inert anodes for the Hall–Héroult process. In the present work, gold, platinum, palladium, copper, tungsten, nickel, cobalt and iron metal electrodes were anodically polarized in an oxide-free cryolite melt (11%wt. excess AlF_3 ; 5%wt. CaF_2) at 1273 K. The aim of the experiments was to characterize the oxidation reactions of the metals occurring without the effect of oxygen-containing dissolved species. The anodic dissolution of each metal was demonstrated, and electrochemical reactions were assigned using reversible potential calculation. The relative stability of metals as well as the possibility of generating pure fluorine is discussed.

1. Introduction

The anodic behavior of metals in molten cryolite mixtures has been investigated for application to inert anodes for the Hall–Héroult process [1]. In traditional cryolite-alumina baths, most of the metal anode materials show a general tendency to oxidize [2]. Although the process depends on the physical and chemical properties of the metal, the reactions involving the anode and dissolved alumina can be represented by the following electrochemical equation:

$$xM_{(s)} + yO^{2-}_{(diss)} = M_xO_{y(s)} + 2ye^- \quad (1)$$

where $O^{2-}{}_{(diss)}$ stands for dissolved oxofluoroaluminates ($AlOF_x^{n-}$) and $M_xO_{y(s)}$ for solid oxide. Precipitation of the oxidation product is likely to occur at the electrode-melt interface, particularly in the case of transition metal oxides which exhibit low solubility [3]. For instance, a copper electrode polarized in an alumina saturated bath was shown to form a passivation layer made of Cu_2O and CuO [4]. The oxidation process of nickel and tungsten has also been established [5], while hematite-based oxide layer formation has been reported on various Fe-Ni alloys [6].

If the metal phase is noble enough, oxygen evolution occurs without involving the electrode material according to:

$$2O^{2-}_{(diss)} = O_{2(g)} + 4e^- \quad (2)$$

Platinum was found to behave as a so-called inert anode and has been used to study oxygen evolution [7]. The reversible potential of the cell $Al_{(l)}/Na_3AlF_6 + Al_2O_{3(sat)}/O_{2(g)}$, Pt was determined to be $E = 2.20$ V at 1273 K. Nevertheless, the anodic dissolution of platinum was found to occur for an overvoltage of about 1 V.

As pointed out by Danek [8], the case of oxide-free cryolite melts has not been investigated to any extent. Reactions involving oxofluoroaluminate species do not occur and reactions like (1) and (2) involving fluoroaluminate species (AlF_x^{n-}, noted $F^-_{(diss)}$) are expected.

Metal phase oxidation might tend to yield fluoride compounds:

$$M_{(s)} + zF^-_{(diss)} = MF_{z(s,l,g)} + ze^- \quad (3)$$

Since no studies have been published about this kind of reaction, different possibilities have to be examined concerning the behavior of the fluorides generated. Precipitation of solid fluoride species MF_z should actually lead to anode passivation, while gaseous or liquid fluoride formation could result in quantitative dissolution of the electrode according to Faraday's law.

An inert anode with respect to fluorine evolution could also be envisaged, resulting in the following reaction:

$$2F^-_{(diss)} = F_{2(g)} + 2e^- \quad (4)$$

However, even though fluorine evolution coupled with oxygen evolution has been proposed on platinum and gold electrodes in cryolite–alumina melts [9], no evidence of the existence of a material capable of supporting pure fluorine evolution has ever been mentioned.

Coupled with cathodic aluminium reduction, the assumed cell reaction would be:

$$AlF_{3(diss)} = \tfrac{3}{2} F_{2(g)} + Al_{(l)} \quad (5)$$

According to thermodynamic data [10], the standard reversible potential for reaction (5) is calculated to be $E° = 4.07$ V vs Al/AlF_3 at 1273 K, which is 1.87 V higher than the standard reversible potential for alumina decomposition.

In the present work, gold, platinum, palladium, copper, tungsten, nickel, cobalt and iron anodes were polarized in an oxide-free cryolite melt at 1273 K. The aim of the experiments was to characterize oxidation reactions occurring without the effect of oxygen-containing dissolved species. The relative stability of the metals as well as the possibility of fluorine discharge is discussed.

2. Experimental

2.1. *The cell*

The cryolite melt was contained in a vitreous carbon crucible, placed in a graphite liner protecting the inside wall of a cylindrical vessel made of refractory steel. The cell was closed by a stainless steel lid cooled by circulating water. A scheme of the experimental setup has been presented elsewhere [11].

The atmosphere was U-grade (less than 5 ppm O_2) inert argon dehydrated with a purification cartridge (Air Liquide). An absolute pressure of around 1.3 atm was maintained during the runs.

2.2. *Chemicals and bath preparation*

The cryolite melt consisted of pure Na_3AlF_6 (Cerac, purity 99.5%), with an 11%wt. excess of AlF_3 (Acros, purity 99.9+%) and a 5%wt. excess of CaF_2 (Merck, purity 99.95%), leading to a cryolite ratio (CR) of 2.2. An oxygen content of 0.1%wt. was measured in the raw powders by LECO analysis: initial alumina content in the melt was under 0.21%wt. The melting point was calculated to be 975 °C [12].

Two-hundred grams of the mixture were placed in the cell, heated to 773 K and dehydrated under vacuum (10^{-5} atm) for 24 h. A temperature of 1273 K was maintained for electrochemical experiments. Careful electrolysis of the bath was then performed using a graphite rod (5 mm diameter) as described in [13]. Low current densities were applied for at least 24 h, to eliminate traces of oxide in the melt.

2.3. *Electrodes*

Metal wires used as anodes were supplied by Goodfellow. Diameters were either 0.5 mm (gold, platinum, and palladium) or 1.0 mm (copper, iron, tungsten, nickel and cobalt). The electrodes were dipped 5–10 mm into the molten salt. The actual immersed height was determined at the end of the run.

The auxiliary electrode was an 8.0 mm diameter graphite rod (Carbone Lorraine), hence with a larger surface area (2.5 cm^2) than the working electrodes.

Potentials were measured with respect to a platinum wire immersed in the bath and acting as a comparison electrode. Its potential was found to be stable after bath electrolysis, due to the reaction of platinum with dissolved aluminium leading to the formation of a Pt–Al alloy [2]. The platinum electrode potential was related to the aluminium deposition potential by cathodic polarization of a tungsten electrode [14].

2.4. *Equipment*

The furnace was built by AET and used Eurotherm thermoregulation. Cyclic voltammetry, linear sweep voltammetry and steady state polarisation were carried out using an Autolab PGSTAT10 potentiostat controlled by GPES software. Scanning electron microscope (SEM) observations were made on a LEO 435 VP. A back-scattered electron (BSE) detector was also used.

3. Results

3.1. *Coulometry and SEM observation of a nickel electrode*

Potensiostatic polarization was performed on a nickel electrode in the oxide-free cryolite melt. The potential value is chosen so that the initial current density is around 1 A cm^{-2}. Figure 1 shows the variation of current density with time for an applied potential of 1.60 V over 300 s. Current density was found to remain stable over the duration of the run, indicating that no passivation of the metal electrode occurs.

SEM observation of a cross section of the nickel electrode after polarization is presented in Figure 2. Dissolution of the metal is clearly confirmed, since the electrode diameter is strongly reduced. Careful examination of the melt–metal interface with the back scattered electron (BSE) detector showed no passivation layer (Picture B).

Similar results were obtained on copper and gold electrodes polarized at 2.10 V and 3.40 V vs Al/AlF_3 respectively.

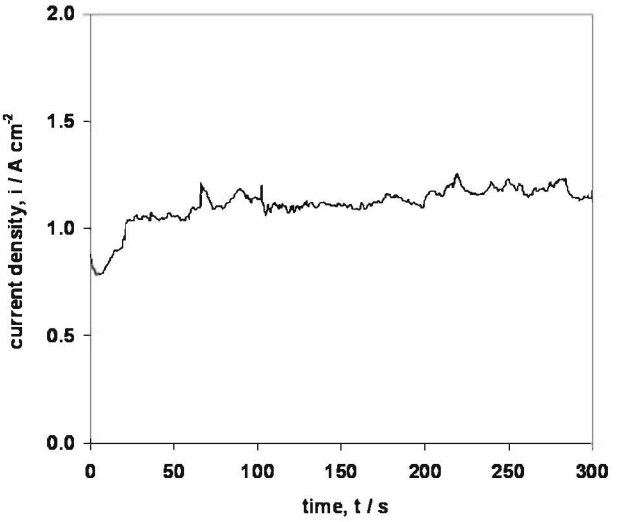

Fig. 1. Potentiostatic polarization ($E = 1.60$ vs Al/AlF_3) of Ni electrode in oxide-free cryolite melt [CR = 2.2; 5%wt. CaF_2; $T = 1273$ K].

3.2. *Linear sweep voltammetry*

Linear sweep voltammetry was performed on cobalt, copper, iron, nickel, tungsten, palladium, platinum and gold electrodes in the oxide-free cryolite bath. The anodic potential was slowly increased (sweep rate 0.002 V s^{-1}) from the open circuit potential up to high density currents, typically higher than 2 A cm^{-2}. The set of curves is presented in Figure 3.

All the materials studied exhibited the same general behavior. When the potential of the metal was kept below a certain value, E_M, specific to each metal investigated, the current density remained very low, indicating an absence of electrode reaction. Then, when the anodic potential reached E_M, the current density increased sharply, with no limiting current. Figure 3 shows that, among the metals studied, iron was the easiest material to oxidize, while gold was the most stable.

The polarization curves were then fitted using Tafel plots in the range $E > E_M$ for each of the eight metals. A good correlation was obtained for Tafel lines, as detailed in Table 1: for all the metals studied, a one-step mechanism controlled by electron transfer predominates over a large potential range. The reaction taking place at the anode was not limited by mass transport, indicating that oxidation products are easily dissolved in the electrolyte. This confirms the SEM observations showing fast dissolution of the anodes.

3.3. *Cyclic voltammetry on gold electrode*

Cyclic voltammetry was performed on a gold electrode in order to identify the anodic reactions occurring on the most stable metal in cryolite. Figure 4 shows voltammograms obtained for sweep rates between 0.1 and 5.0 V s^{-1}. A reverse potential scan was applied from the open circuit potential (~0.70 V vs ref.) up to the anodic dissolution wave, noted O2.

In addition, the whole electrochemical window was examined on a cyclic voltammogram with a sweep rate of 0.2 V s^{-1}. The cathodic limit (R1) is located at a potential of around 0.35 V vs Al/AlF_3. A similar electrochemical window was observed by Duruz et al. [15], and reaction (R1) was attributed by the authors to low melting Au–Al–Na alloy formation.

An oxidation reaction (O1) is observed before anodic dissolution of the gold electrode, in the potential range 2.20–2.70 V vs Al/AlF_3. Current densities of anodic peaks are plotted in Figure 5 versus the square root of the potential sweep rate: the linear relationship confirms that a mass-transport controlled reaction occurs at the electrode. Diffusion-limited oxygen evolution due to oxidation of residual dissolved alumina is the most probable assumption to explain this reaction.

The high cathodic currents during the reverse sweep indicate that reaction (O2) yields dissolved species. If the product were gaseous, the gas would escape from the electrode diffusion layer, and no reverse reaction would be observed. If the oxidation product was a solid, the ratio of charge density between anodic and cathodic reactions would be close to one, while in this case, a ratio of around 0.5 was measured from integration of the voltammograms for sweep rates between 0.5 and 5.0 V s^{-1}.

It can be concluded therefore that gold is anodically dissolved in the cryolite melt at a potential of around one volt more anodic than oxygen discharge.

4. Discussion

The dissolution potentials E_M were measured for each metal by intersection of the anodic branch of the

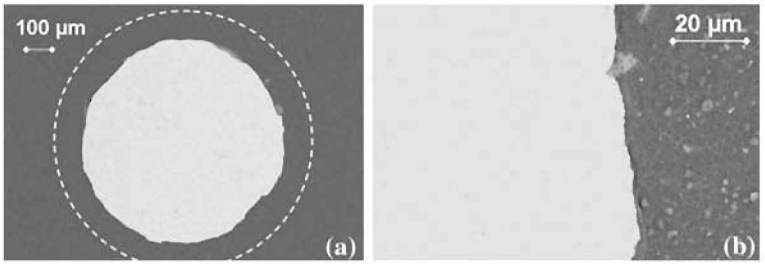

Fig. 2. SEM-BSE observation of a nickel electrode after potentiostatic polarization (a) dotted line represents the initial diameter (1 mm) (b) close up on the interface.

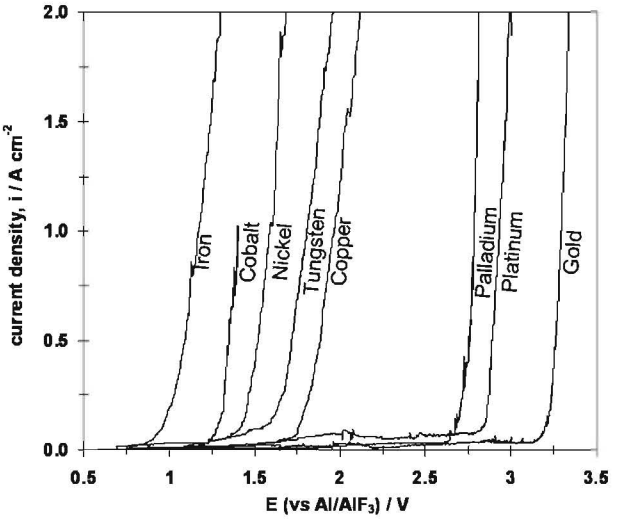

Fig. 3. Steady state current versus potential (0.002 V s^{-1}) curves on metal electrodes in oxide-free cryolite melt [CR = 2.2; 5%wt. CaF_2; $T = 1273$ K].

Table 1. Tafel slopes measured on linear sweep voltammograms in oxide-free cryolite melt. R^2: correlation coefficient

Metal	Tafel slope/V $(dec)^{-1}$	R^2
Gold	0.105	0.990
Platinum	0.089	0.983
Palladium	0.111	0.985
Copper	0.177	0.983
Tungsten	0.258	0.984
Nickel	0.195	0.982
Cobalt	0.117	0.979
Iron	0.209	0.990

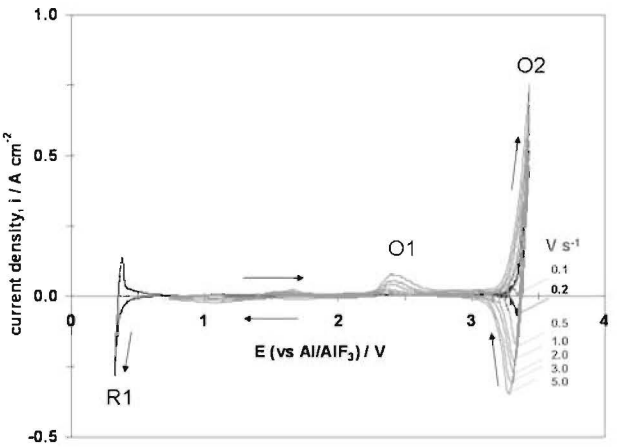

Fig. 4. Cyclic voltammetry on gold electrode in oxide-free cryolite melt. Sweep rates: 0.1, 0.2, 0.5, 1.0, 2.0, 3.0, 5.0 V s^{-1}. R1: reduction reaction; O1 and O2: oxidation reactions.

voltammogram with the x-axis in Figure 3. Potential values are reported in Table 2.

Since the measured potentials are expressed versus the Al/AlF_3 reference, the appropriate cell reaction leading to the formation of fluorides is:

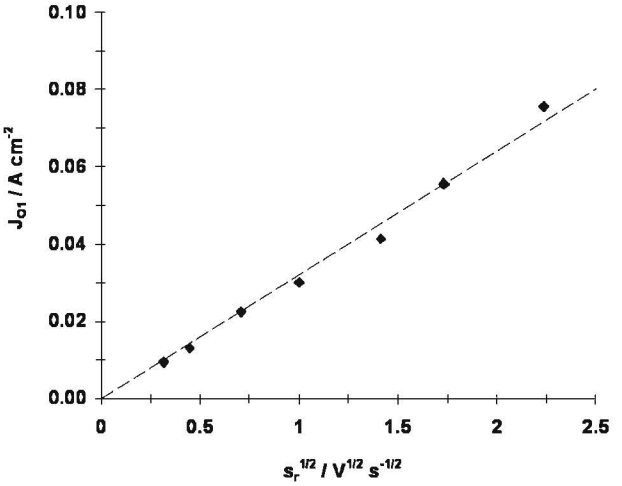

Fig. 5. Linear relationship of oxidation peak vs. the square root of potential sweep rate for reaction O1 on gold electrode.

$$M_{(s)} + \frac{z}{3}AlF_{3(diss)} = MF_{z(s,l,g)} + \frac{z}{3}Al_{(l)} \quad (6)$$

In order to assign reactions to the dissolution curves, the reversible potentials related to equation (6) were calculated according to the Nernst equation:

$$E_{(M/MF_z)} = E^\circ + \frac{2.303RT}{zF}\log\left[\frac{a(MF_z)a(Al)^{z/3}}{a(M)a(AlF_3)^{z/3}}\right] \quad (7)$$

where: activities of pure phases Al and M (a(Al) and a(M)) are equal to unity, the activity of AlF_3 in the melt (CR = 2.2 + 5%wt CaF_2) is $a(AlF_3) = 0.0025$ according to [16], standard potential E° is defined as $\Delta_r G^\circ(T) = zFE^\circ$ ($\Delta_r G^\circ(T)$ is the standard free enthalpy of reaction (6)). The reversible potential is then expressed versus the Al/AlF_3 electrochemical reference [2].

At 1273 K, Equation (7) can be expressed as:

$$E_{(M/MF_z)} = \frac{\Delta_r G^\circ_{(1273\,K)}}{zF} + \frac{0.252}{z}\log[a(MF_z)] + 0.219 \quad (8)$$

Table 3 reports the reversible potentials calculated from equation (8) for the eight metals studied. Since the activity of MF_z fluorides dissolved in the melt are not known, $a(MF_z)$ was assumed to equal unity. Data from Barin [10] were used for $\Delta_r G^\circ$ calculations. As mentioned in Table 3, some data concerning fluorides had to be extrapolated to 1273 K.

In most cases, as several oxidation states exist, various reactions of the metal phase are possible. The lowest reversible potential means that reaction is thermodynamically favored, and hence determines which fluoride is the most likely to form. With the exception of gold and tungsten, the lowest oxidation state was found to be the most stable.

Table 2. Dissolution potential of metals measured in oxide-free cryolite melt at 1273 K

Metal	Dissolution potential (vs Al/AlF_3)/V
Gold	3.20
Platinum	2.85
Palladium	2.65
Copper	1.75
Tungsten	1.60
Nickel	1.40
Cobalt	1.25
Iron	0.85

These calculations were then compared to electrochemical measurements, and M/MF_z couples were assigned as illustrated in Figure 6.

First, it should be noted that the calculated relative stability of the metals was similar to the experimental measurements, except in the case of tungsten. Indeed, thermodynamic data for $WF_{4(g)}$ were extrapolated from 500 K (Table 3), so calculation might be erroneous. Formation of $WF_{6(g)}$ at $E = 1.96$ V/ref. would be in better agreement with the measured relative stability.

Another observation is that all the measured potentials were smaller by 0.10 to 0.70 V than the calculated ones. The smallest difference was observed for gaseous fluorides $WF_{4(g)}$ and $PtF_{4(g)}$, with a variation of 0.17 and 0.10 V, respectively, between experiment and calculation. The most credible explanation is that the activity coefficients of dissolved species are lower than one. Indeed, equation (8) shows that the reversible potential decreases by $-0.252/z$ V per decade with decreasing fluoride species activity.

Dissolved AlF_3 has an activity of 0.0025 in the melt [16]. Similarly, complexation by the ionic salt is likely to lower the activity of the dissolved fluoride and, hence, the reversible potential of the reaction.

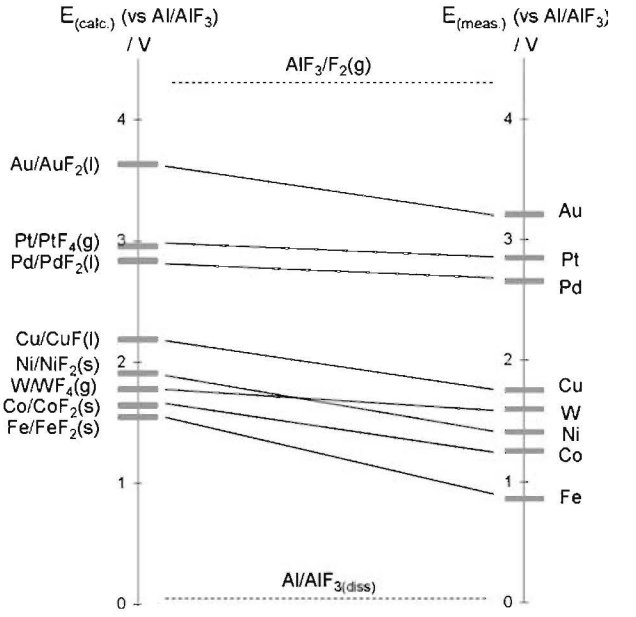

Fig. 6. Comparison between measured and calculated reversible potentials for reaction (6) in oxide-free cryolite melt at 1273 K.

Both experiment and calculation demonstrate that fluorine evolution on a metal anode is not possible without rapid dissolution of the anode material. Indeed, the gold electrode, which was found to be the most stable element, started dissolving at 3.20 V vs Al/AlF_3. This potential is about one volt lower than the calculated potential for fluorine evolution. Simple extrapolation using the Tafel slope for a gold electrode ($+0.10$ V $(dec)^{-1}$) indicates that a current density of 10^{10} A cm^{-2} would be necessary to promote fluorine discharge.

Other anode materials are also unlikely to support fluorine discharge. Indeed, with carbon materials there is an anode effect due to CF_x formation [2], while oxide materials are expected to decompose in low alumina-content melts according to [17]:

Table 3. Calculated reversible potentials for reaction $M_{(s)} + \frac{z}{3}AlF_{3(diss)} = MF_{z(std)} + \frac{z}{3}Al_{(l)}$ at 1273 K with a $(MF_z) = 1$ and $a(AlF) = 0.0025$. Data for fluorides MF_z are extrapolated from T_{extr}. z is the oxidation state

Metal	Possible reactions	z	T_{extr}/K	$\Delta_r G°$/kJ mol^{-1}	E(vs Al/AlF_3)/V
Gold	$Au_{(s)} + 1/3\ AlF_{3(diss)} = AuF_{(g)} + 1/3\ Al_{(l)}$	I	398	387	4.24
	$Au_{(s)} + 2/3\ AlF_{3(diss)} = AuF_{2(l)} + 2/3\ Al_{(l)}$	II		712	3.62
	$Au_{(s)} + AlF_{3(diss)} = AuF_{3(l)} + Al_{(l)}$	III	600	1101	4.02
Platinum	$Pt_{(s)} + 4/3\ AlF_{3(diss)} = PtF_{4(g)} + 4/3\ Al_{(l)}$	IV	500	1049	2.94
	$Pt_{(s)} + 2\ AlF_{3(diss)} = PtF_{6(g)} + 2\ Al_{(l)}$	VI	398	2073	3.80
Palladium	$Pd_{(s)} + 2/3\ AlF_{3(diss)} = PdF_{2(l)} + 2/3\ Al_{(l)}$	II	1100	503	2.82
Copper	$Cu_{(s)} + 1/3\ AlF_{3(diss)} = CuF_{(l)} + 1/3\ Al_{(l)}$	I		1089	2.18
	$Cu_{(s)} + 2/3\ AlF_{3(diss)} = CuF_{2(l)} + 2/3\ Al_{(l)}$	II		426	2.42
Tungsten	$W_{(s)} + 1/3\ AlF_{3(diss)} = WF_{(g)} + 1/3\ Al_{(l)}$	I		637	6.82
	$W_{(s)} + 4/3\ AlF_{3(diss)} = WF_{4(g)} + 4/3\ Al_{(l)}$	IV	500	592	1.75
	$W_{(s)} + 5/3\ AlF_{3(diss)} = WF_{5(g)} + 5/3\ Al_{(l)}$	V	500	1106	2.51
	$W_{(s)} + 2\ AlF_{3(diss)} = WF_{6(g)} + 2\ Al_{(l)}$	VI		1009	1.96
Nickel	$Ni_{(s)} + 2/3\ AlF_{3(diss)} = NiF_{2(s)} + 2/3\ Al_{(l)}$	II		324	1.88
Cobalt	$Co_{(s)} + 2/3\ AlF_{3(diss)} = CoF_{2(s)} + 2/3\ Al_{(l)}$	II		273	1.63
	$Co_{(s)} + AlF_{3(diss)} = CoF_{3(l)} + Al_{(l)}$	III	1200	678	2.56
Iron	$Fe_{(s)} + 2/3\ AlF_{3(diss)} = FeF_{2(s)} + 2/3\ Al_{(l)}$	II		254	1.54
	$Fe_{(s)} + AlF_{3(diss)} = FeF_{3(g)} + Al_{(l)}$	III		422	1.60

$$M_xO_y + 2yF^-_{(diss)} = \frac{y}{2}O_{2(g)} + xMF_{\frac{2y}{x}(s,l,g)} + 2ye^- \quad (9)$$

For instance, a decomposition potential of about 2.50 V was measured with tin oxide at 1030 °C [18].

5. Conclusion

The study of the anodic polarization of eight metals in oxide-free cryolite melts yields relevant information on the oxidation reactions occurring at metal electrodes. The anodic dissolution of each metal was demonstrated, and linear voltammetry allowed a scale to be built indicating the relative stability of the metals. Gold is the most stable, followed by platinum, palladium, copper, tungsten, nickel, cobalt and iron. The first three metals exhibit a dissolution potential higher than the oxygen evolution potential, while the others dissolve at a potential under 2.20 V vs Al/AlF_3.

In cryolite melts, evolution of fluorine at metal anodes seems to be impossible without their rapid dissolution. Since neither carbon nor oxide materials allow fluorine to be evolved under polarisation, it is concluded that no anode material is suitable for this reaction.

Acknowledgements

The authors thank L. Massot (Laboratoire de Génie Chimique, Toulouse) for SEM imaging.This work was supported by Aluminium Pechiney and French "Ministère de l'Economie, des Finances et de l'Industrie".

References

1. R.P. Pawlek, in J. Anjier (Ed), 'Inert Anodes: An Update, in Light Metals, proceedings of TMS Annual Meeting', (Charlotte, North Carolina, March 14–18, 2004), pp. 283–287.
2. J. Thonstad, P. Fellner, G.M. Haarberg, J. Hives, H. Kvande and Å. Sterten, *Aluminium Electrolysis, Fundamentals of the Hall–Héroult Process*, 3rd ed, (Aluminium-Verlag, Düsseldorf, 2001).
3. K. Billehaug and H.A. Øye, *Aluminium* **57** (1981) 146.
4. C.F. Windisch and S.C. Marschman, in R.D. Zabreznik (Ed), 'Electrochemical Polarization Studies on Cu and Cu-Containing Cermet Anodes for the Aluminum Industry, in Light Metals, proceedings of TMS annual meeting', (Cincinnati, Ohio, 1987), pp. 351–355.
5. S.S. Djokic and B.E. Conway, *J. Appl. Electrochem.* **25** (1995) 106.
6. J.J.R. Duruz and V. de Nora, Cells for the Electrowinning of Aluminium Having Dimensionally Stable Metal-Based Anodes, WO patent 00/06,803 (1999).
7. J. Thonstad, *Electrochim. Acta* **13** (1968) 449.
8. V. Danek, M. Chrenková and A. Silný, *Coord. Chem. Rev.* **167** (1997) 1.
9. E.W. Dewing and E.T.v.d. Kouwe, *J. Electrochem. Soc.* **124** (1) (1977) 58.
10. I. Barin, O. Knacke and O. Kubashewski, *Thermochemical Properties of Inorganic Substances* (Springer-Verlag, Berlin, 1991).
11. P. Chamelot, B. Lafage and P. Taxil, *J. Electrochem. Soc.* **143** (5) (1996) 1570.
12. A. Solheim, S. Rolseth, E. Skybakmoen, L. Stoen, Å. Sterten and T. Store, *Metall. Mater. Trans. B* **27** (1996) 739.
13. J. Thonstad, F. Nordmo and J.K. Rodseth, *Electrochim. Acta* **19** (1974) 761.
14. W.E. Haupin, *JOM-J MIN MET MAT S* **23** (1971) 46.
15. J.J. Duruz, G. Stehle and D. Landolt, *Electrochim. Acta* **26** (6) (1981) 771.
16. A. Solheim and Å. Sterten, *in* C.E. Eckert (Ed), 'Activity of Alumina in the System $NaF–AlF_3–Al_2O_3$ at NaF/AlF_3 Molar Ratios Ranging from 1.4 to 3, in Light Metals, proceedings of TMS annual meeting', (San Diego, California, February 27–March 4, 1999) pp. 445–452.
17. S.P. Ray, *in* R.D. Zabreznik (Ed), 'Effect of Cell Operating Parameters on Performance of Inert Anodes in Hall–Héroult Cells, in Light Metals, Proceedings of TMS Annual Meeting', (Cincinnati, Ohio, 1987) pp. 367–380.
18. H. Xiao, On the Corrosion and the Behaviour of Inert Anodes in Aluminium Electrolysis, PhD Thesis (NTNU, Trondheim, 1993).